Supporting On-line Material

Materials: GTP, GDP, xanthine, xanthine oxidase, imidazole cellulose PEI matrix TLC plates, Lucigenin, β-NADPH and E. Coli manganese superoxide dismutase were purchased from Sigma-Aldrich corporation (St. Louis, MO). Dulbecco's modified Eagle's medium (DMEM), penicillin/streptomycin (P/S), 0.25% trypsin-EDTA, fetal bovine serum (FBS), Amphotericin B and collagenase were purchased from Invitrogen corporation (Carlsbad, CA). Radioactive nucleotides, liquid scintillation fluid and nitrocellulose protein transfer membrane were purchased from Amersham Biosciences (Piscataway, NJ). Protease inhibitor cocktail (PIC), EDTA-free PIC, GTPγS and GDPβS were purchased from Roche Applied Science (Indianapolis, IN). Histidine-tagged Rac1 (His-Rac1), His-Cdc42 and Glutathione transferase-tagged (GST) p50-Rho-GAP catalytic domain (p29-GAP) were purchased from Cytoskeleton Inc. (Denver, CO). Bovine copper/zinc superoxide dismutase (SOD1) was purchased from Oxis Research (Portland, OR). Dynabeads talon, dynabeads protein-A and protein-G were purchased from Dynal Biotech (Lake Success, NY). Iodixanol was purchased from Accurate Chemical & Scientific Corp. (Westbury, NY).

Rac1-activation assays: Rac1 activation assays were performed using a previously described protocol with modifications (1). Briefly, this assay utilizes a GST-PBD binding domain (Cytoskeleton) of PAK to specifically bind GTP-Rac1 (PBD encodes the p21 binding domain of PAK1). Tissue or cell lysates were normalized for protein concentration using the Bradford assay. GTP-bound Rac1 was precipitated from 1 mg of whole cell or tissue lysate with GST-PBD using protein G dynabeads conjugated with anti-GST antibody. The immunoprecipitated pellet was evaluated by Western blotting for Rac1. The intensity of Rac1 immunoreactivity correlates with the level of GTP-bound Rac1 in the sample.

Guanine Nucleotide Exchange (GEF) Assay: GEF activity was assayed as previously described (2) by measuring the incorporation of ^{35}S-GTPγS into purified His-tagged Rac1. Briefly, 1 μCi of ^{35}S-GTPγS was incubated with 250 picomoles His-tagged Rac1 in the presence or absence of 750 picomoles purified bovine SOD1 at 30°C for 30 min with gentle agitation in GEF buffer containing 25 mM Tris-HCl, pH 8.0, 1 mM dithiothreitol, 5 mM EDTA, and 10 mM $MgCl_2$. The samples were filtered through nitrocellulose membrane and washed four times with washing buffer containing 25 mM Tris-HCl, pH 8.0, 100 mM NaCl, and 30 mM $MgCl_2$. Incorporated ^{35}S-GTPγS on Rac1 was measured using liquid scintillation spectrometry.

Primary mouse dermal fibroblast (PMDF) isolation: PMDFs were isolated from *Nox2*^{gp91phox}-deficient breeding pairs or congenic wild type C57BL/6 breeding pairs (3). 1-day-old pups were euthanized, cleaned with sterile PBS, and their skins were removed immediately. Skin from each pup was separately placed with the dermal side down into a sterile 35 mm Petri dish and floated on 0.25% trypsin-EDTA overnight in 4°C. The following day, the epidermis was peeled off the dermis. The dermis was then incubated in 0.2% collagenase in DMEM for 1 hour at 37°C. The dermis was shaken to release the fibroblasts, this mixed cell population was pelleted and plated in DMEM with 10% FBS, 1% P/S, 2.5 units/ml Amphotericin B, and 2 mM L-Glutamine. Calcium was raised to 6 mM to induce calcium-dependent differentiation and detachment of contaminating keratinocytes. Following expansion of PMDFs, genomic DNA was generated from a subset of cells from each isolate for *Nox2* genotyping.

Primary mouse embryonic fibroblast (PMEF) isolation: PMEFs were isolated from breeding pairs of mice heterozygous for targeted disruption of endogenous mouse *SOD1* (4). Embryos were harvested from 14-day post coitus pregnant female mice. Following removal of the head and internal organs, embryos were rinsed in PBS, minced and incubated in 0.25% trypsin-EDTA overnight in 4°C. Trypsin was inactivated by adding DMEM with 10% FBS, 1% P/S, 2 mM L-Glutamine, and 55 μM β-mercaptoethanol. The cells were washed and plated in the same media. Following expansion of PMEFs, genomic DNA was generated from a subset of cells from each isolate for *SOD1* genotyping. PMEFs heterozygous for the *SOD1* gene were used for endosomal isolations to allow for functional complementation by exogenously supplied purified SOD proteins.

Cresyl violet staining of spinal cord and motor neuron counts: Mice were anesthetized deeply with a combination of 150 mg/g ketamine and 15 mg/g xylazine in sterile PBS and perfused transcardially with 20 ml filtered cold PBS followed by 20 ml 4% paraformaldehyde. Spinal cords were harvested and placed into 4% paraformaldehyde and kept at 4ºC overnight. Cords were then stored in sterile PBS at 4ºC for at least 24 hours before cryoprotection in 30% sucrose overnight. The lumbar spinal cord was removed from the remainder of the spinal cord and cut into 4 mm-long segments. Segments were embedded in OTC freezing medium and sectioned axially at 20 μm at -35ºC with a Microm Cryostat II equipped with the Cryo-Jane System (Instrumedics, Inc., Hackensack, NJ) for preservation of tissue structure. Every fifth section was stained with 0.1% (w/v) cresyl violet acetate (Nissl stain) without counterstain (5). Motor neurons in the ventral horn were quantified by counting large pyramidal neurons that stain with cresyl violet and possess a prominent nucleolus. At least 11 sections of spinal cord were counted per mouse and the analysis was blinded. Three animals in each treatment group were analyzed at one time for consistency of staining and quantification.

References:

1. Sanlioglu, S., Williams, C.M., Samavati, L., Butler, N.S., Wang, G., McCray, P.B., Jr., Ritchie, T.C., Hunninghake, G.W., Zandi, E., and Engelhardt, J.F. 2001. Lipopolysaccharide induces Rac1-dependent reactive oxygen species formation and coordinates tumor necrosis factor-alpha secretion through IKK regulation of NF-kappa B. *J Biol Chem* 276:30188-30198.
2. Manser, E., Loo, T.H., Koh, C.G., Zhao, Z.S., Chen, X.Q., Tan, L., Tan, I., Leung, T., and Lim, L. 1998. PAK kinases are directly coupled to the PIX family of nucleotide exchange factors. *Mol Cell* 1:183-192.
3. Pollock, J.D., Williams, D.A., Gifford, M.A., Li, L.L., Du, X., Fisherman, J., Orkin, S.H., Doerschuk, C.M., and Dinauer, M.C. 1995. Mouse model of X-linked chronic granulomatous disease, an inherited defect in phagocyte superoxide production. *Nat Genet* 9:202-209.
4. Matzuk, M.M., Dionne, L., Guo, Q., Kumar, T.R., and Lebovitz, R.M. 1998. Ovarian function in superoxide dismutase 1 and 2 knockout mice. *Endocrinology* 139:4008-4011.
5. Vopicelli-Daley, L.A.a.A.L. 2003. Immunohistochemical localization of proteins in the nervous system. In *Current Protocols in Neuroscience*. Crawley, editor. 1.2.1-1.2.17.

6. Hirshberg, M., Stockley, R.W., Dodson, G., and Webb, M.R. 1997. The crystal structure of human rac1, a member of the rho-family complexed with a GTP analogue. *Nat Struct Biol* 4:147-152.

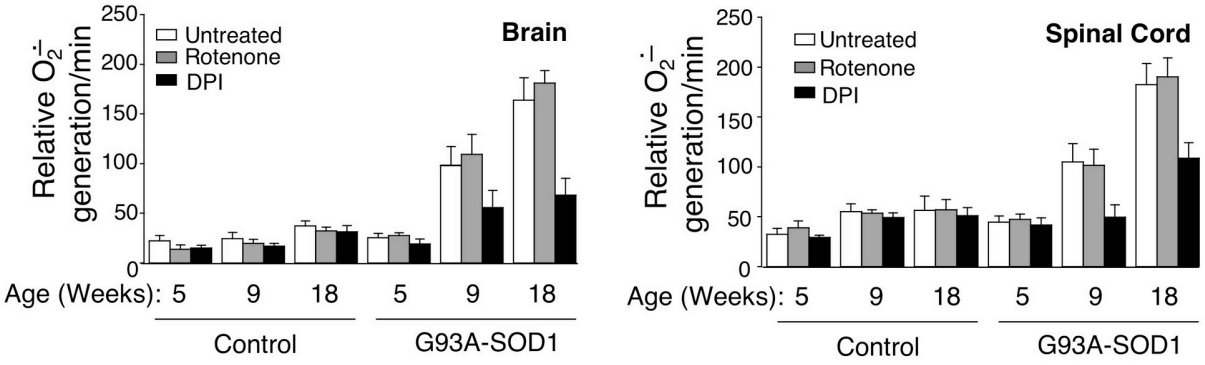

Fig. S1. NADPH-dependent superoxide production by brain and spinal cord endomembranes isolated from non-transgenic (control) and hemizygous *SOD1*^{G93A} transgenic mice. NADPH-dependent superoxide production was measured using the lucigenin assay in the absence or presence of DPI (10 μM) or rotenone (100 μM). DPI was used as a general inhibitor of NADPH oxidases and rotenone was used inhibit mitochondrial respiration. In both tissues, SOD1^{G93A}-induced NADPH-dependent superoxide production at 9 and 18 weeks was significantly inhibited by DPI but not rotenone.

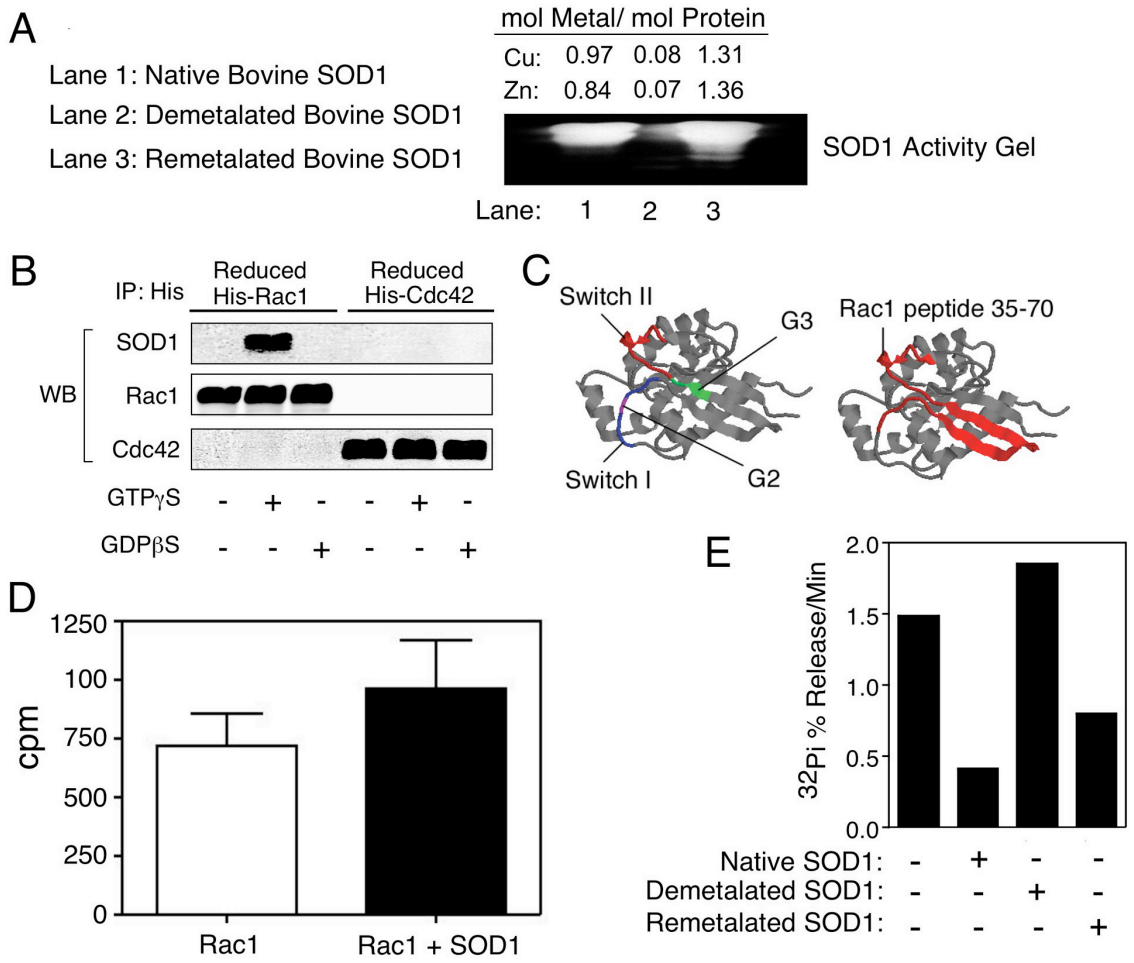

Fig. S2. SOD1 does not affect GTP loading of Rac1 and must be enzymatically active to influence Rac1 GTPase activity. (A) SOD1 activity gel for (lane 1) native bovine SOD1, (lane 2) demetalated bovine SOD1, and (lane 3) remetalated bovine SOD1. Zn and Cu content of each form of bovine SOD1 is given above the gel in moles of metal per moles of protein. (B) In vitro pull-down assays of His-Rac1 or His-Cdc42 pre-reduced with 300 μM DTT, pre-loaded with GTPγS, and then incubated with bovine SOD1 prior to His-precipitation and Western blotting for Rac1, SOD1, and Cdc42. (C) Cartoon of the 3-dimentional structure of the Rac1 polypeptide backbone (6). Left panel demonstrates the switch I region (blue), switch II region (red), G2 region (magenta) and the G3 region (green). Right panel demonstrates the minimal Rac1 peptide that strongly bound SOD1 (red) spanning the switch I, switch II, β1, β2, G2, and G3 regions. (D) Rac-GEF assays were performed by quantifying loading of His-tagged Rac1 with ^{35}S-GTPγS in the presence or absence of bovine SOD1. The proteins were bound to nitrocellulose membrane and the excess unbound radionucleotide was removed by washing. The remaining (bound) ^{35}S-GTPγS was quantified by liquid scintillation spectrometry. Results depict the mean +/-SEM for N=3 independent experiments. (E) Rac1 GTPase assays were performed in the presence or absence of purified native, demetalated, or remetalated bovine SOD1. His-tagged Rac1 was preloaded with γP^{32}-GTP and the rate of ^{32}Pi release from γP^{32}-GTP is plotted. Results are representative of two experiments.

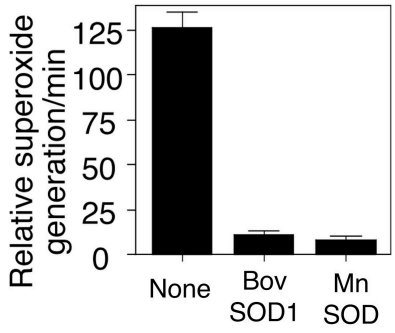

Fig. S3. Both bovine SOD1 and bacterial MnSOD equally scavenge $O_2^{\bullet-}$ despite their different abilities to act as an effector of Rac1. The ability of bovine SOD1 (BovSOD1) and *E.Coli* SOD (MnSOD) to scavenge X/XO-derived $O_2^{\bullet-}$ was evaluated using lucigenin-based chemiluminescent detection of $O_2^{\bullet-}$. A reaction with 50 mU XO and 125 μM Xanthine was initiated in the absence or presence of 2.5 μM SOD and the relative rate of $O_2^{\bullet-}$ production was immediately determined. The mean (+/-SEM) relative rates of X/XO-derived $O_2^{\bullet-}$ are given (n=3).

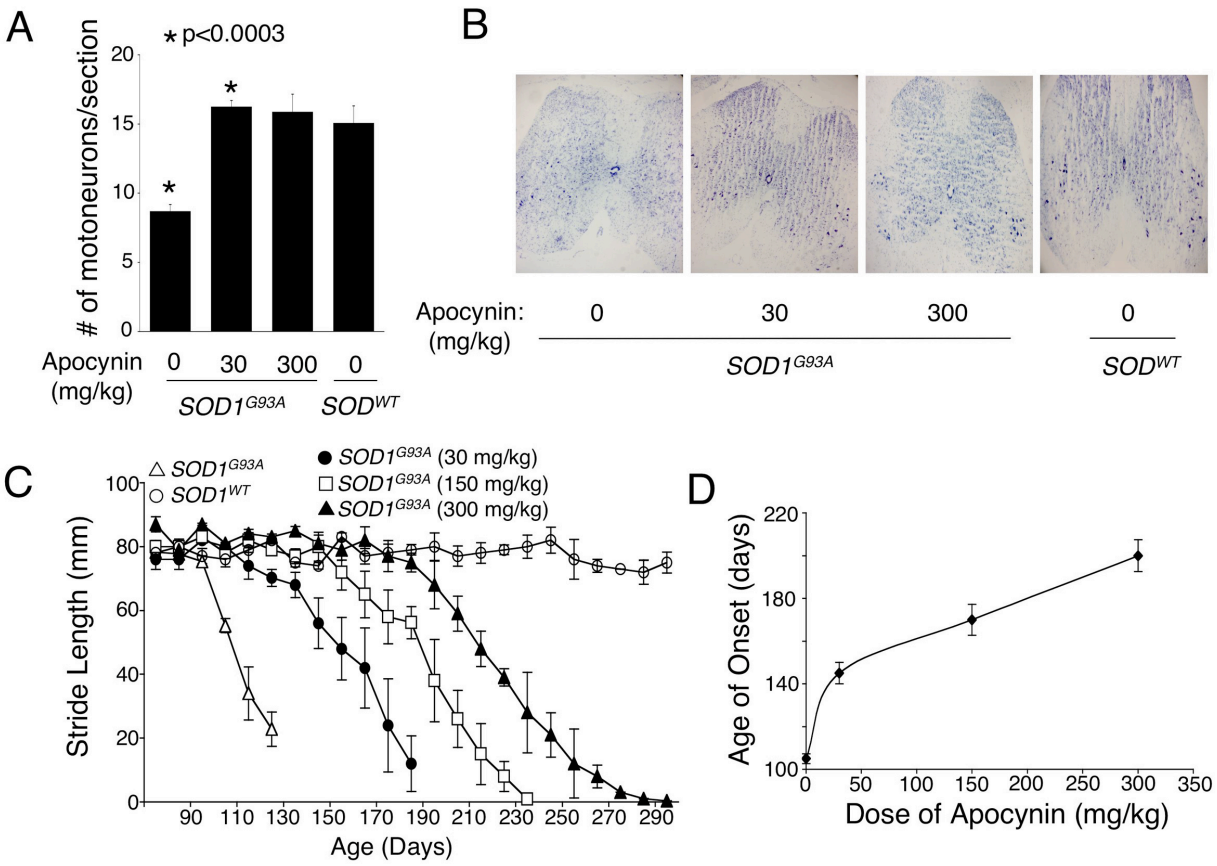

Fig. S4. Treatment of *SOD1*^{G93A} transgenic mice with apocynin reduces motor neuron loss and progression of gait deficiencies. (A) Motor neurons were quantified in the lumbar region of the spinal cord using cresyl violet staining at 120 days for each treatment group. In total three animals were included in each group and quantification was blinded to treatment conditions and genotype. Results depict the mean +/-SEM motor neurons per section for the indicated groups (N=3 in each group). (B) Representative photomicrographs of lumbar spinal cord sections stained in cresyl violet. (C) Stride length data demonstrating the mean stride distance for each dosage group as a function of age in days. (D) The effect of apocynin on age of disease onset as determined by a 25% decline in maximum stride length. Results in (C) and (D) depict the mean (+/-SEM) for the cohort of mice evaluated in Figure 4A in the main text. Statistically differences were seen between all group comparisons in panel (C) and (D).

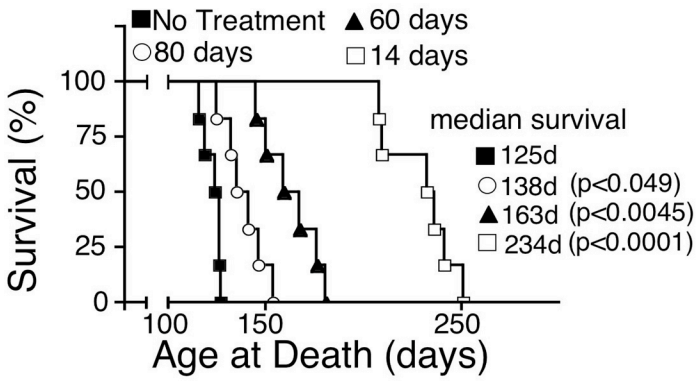

Fig. S5. Therapeutic benefit of treating *SOD1*^{G93A} transgenic mice with apocynin (300 mg/kg) at different ages after birth. Survival times of hemizygous *SOD1*^{G93A} transgenic mice either untreated or given 300 mg/kg apocynin in their drinking water starting at 14, 60 and 80 days of age (N=6 for each group). The p-value to the right of the median survival (days) for each dose is in comparison to untreated controls. The cohort of mice in this study was derived from three transgene negative sibling females and one *SOD1*^{G93A} hemizygous male. Two consecutive litters from each mother were analyzed in the cohort.